Numerical Prediction of Wind Pressure Around a High-Rise Residential Building in an Urban Area Using Large Eddy Simulation Based on the Lattice Boltzmann Method

Yoshiaki ITOH[a], Kouji KONDO[a], Tetsuro TAMURA[b], Koichi IJUIN[c]

[a]Kajima Technical Research Institute, 2-19-1 Tobitakyuu, Chofu-shi, Tokyo, itohyoshiaki@kajima.com
[b]Yokohama National University, 79-2 Tokiwadai, Hodogaya-ku, Yokohama, Kanagawa, Japan
[c]Altair Engineering, 2-2-1 Kyobashi, Chuou-ku, Tokyo

We performed a Large Eddy Simulation (LES) of the flow around a high-rise residential building featuring double corner recesses and chamfered corners in a boundary layer wind tunnel. We used the D3Q27 cumulant Lattice Boltzmann Method (LBM) incorporating a LBM-consistent Smagorinsky subgrid-scale model and a turbulent boundary layer equation–based wall model on a Cartesian mesh with octree-based grid refinement. The rough-wall turbulent boundary layer with a power index of 0.2 was successfully reproduced. The mean, standard deviation and maximum and minimum peak wind pressure coefficients obtained by the LBM for the target building in cases with a wind angle of 80° and 90° were found to be within approximately ±20% of the experimental results.

Keywords: Large eddy simulation (LES), lattice Boltzmann method (LBM), peak wind pressure, high-rise residential building, corner recesses, chamfered corners, boundary layer wind tunnel

1. Introduction

To ensure the safety of buildings subjected to strong winds, it is necessary to evaluate the wind pressures and forces induced by turbulent flows at ground level. Computational fluid dynamics (CFD) is often used instead of conventional wind tunnel experiments for these evaluations. However, because an accurate assessment requires resolving instantaneous fluctuations in wind pressure and force, Reynolds-Averaged Navier–Stokes (RANS) models are insufficient, and Large Eddy Simulation (LES) is required. In LES-based wind-resistant design, the incompressible Navier–Stokes and continuity equations are discretized and solved using numerical methods such as the finite volume method. Guidelines specifying computational methodologies and conditions to ensure engineering reliability have been established, and computational accuracy has been validated through comparisons with wind tunnel experimental results [1,2, and 3].

In recent years the lattice Boltzmann method (LBM) has emerged as an alternative approach to analyzing fluid flow. In LBM, fluid motion is modeled by the streaming and colliding particle distribution functions. The time evolution of these distributions is computed on a uniform Cartesian grid. Because LBM employs an explicit numerical scheme and is well suited for large-scale parallel computation, it is expected to enable the efficient LES of flows around real buildings with complex geometries. However, few studies have evaluated peak wind pressure coefficients to access wind loads on building cladding in turbulent boundary layers using LBM [4]. Accordingly, this study performs LES of a high-rise residential building located in an urban area. The analysis is based on wind pressure measurements conducted under the Building Standard Development Promotion Program of the Ministry of Land, Infrastructure, Transport and Tourism [3,5]. The objective is to evaluate the computational accuracy and efficiency of the proposed approach.

2. Analysis model and wind tunnel experiment for accuracy verification

The analysis target is a high-rise residential building with a height $H = 128$ m and a frontage width $B = 43$ m. The building features double corner recesses, chamfered corners, and external balconies. The surrounding urban area within a 400-m radius of the target building, consisting of low- and mid-rise buildings (i.e., surrounding city blocks), is also included in the analysis (see Figure 1). Figure 2 shows the floor plan of the upper stories. From 106 to 128 m (roof level), the building incorporates double corner recesses. Between heights of 67.5 and 106 m, the corners are chamfered. Below 67.5 m, external balconies are present down to a height of 8 m. From 8 m to ground level, the building has a square plan, with a canopy located at the center of the north facade.

As the computational model, the entire test section of the general-purpose boundary layer wind tunnel at the Kajima Technical Research Institute, which was used in previous CFD validation studies [3,5], was reproduced as the LES computational domain (see Figure 3). A turbulent boundary layer was generated in the test section using spires, roughness blocks, and barriers that were identical in shape and arrangement to those in the physical wind tunnel. This produced inflow turbulence that corresponded to terrain category III (power-law exponent 0.2), as defined in *Recommendations for Loads on Buildings* (2015) [6]. The wind tunnel model was constructed at a scale of 1:400. To validate the accuracy of the computational model for LBM, two wind directions were considered: 90°, which corresponds to a flow normal to the east facade of the building, and 80°, which represents a slight deviation from normal incidence, at which the absolute value of the negative peak pressure at the windward corner is maximized.

A uniform inflow with a velocity of 12.1 m/s was imposed at the inlet boundary (see Figure 3). This resulted in a reference wind velocity $U_H = 10$ m/s at the height of the model building (0.32 m). Wind pressure coefficients at the measurement points were recorded at a sampling frequency of 1000 Hz. To evaluate the peak (maximum and minimum) wind pressure coefficients, we considered the scale effects of exterior cladding materials. Peak values were determined using the time-varying load method, with an averaging time equivalent to 0.45 s at full scale (implemented as a moving average over five consecutive data points). The analysis was conducted over a data duration equivalent to 10 min at full scale, followed by ensemble averaging. The number of ensembles was nine for the wind tunnel experiments and five for the LES.

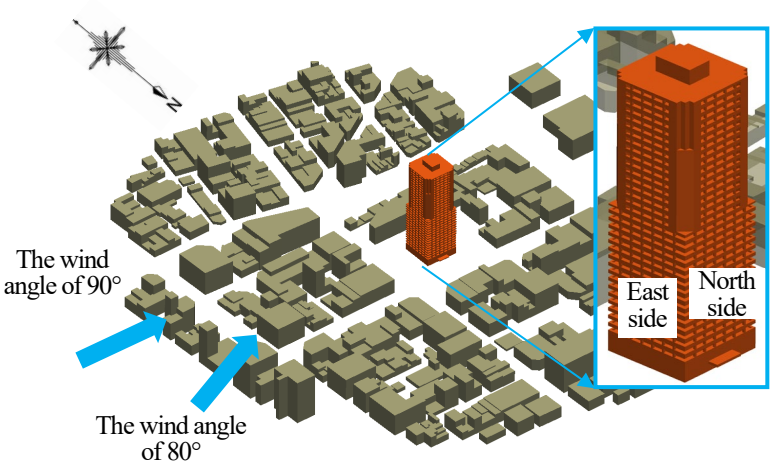

Fig. 1. Model of the high-rise residential building in an urban area.

3. Computational method

LES based on the LBM was performed using the commercial software Altair ultraFluidX [7,8]. The solver is based on the cumulant Lattice Boltzmann formulation proposed by Martin Geier [9–11], and incorporates an equivalent standard Smagorinsky subgrid-scale model [12] and wall modeling [13]. The D3Q27 lattice model was used to discretize the three-dimensional velocity space. To represent complex geometries, a Cartesian mesh with octree-based grid refinement (with grid spacing reduced by a factor of 0.5 between successive levels) was adopted. An immersed boundary method based on a one-dimensional turbulent boundary layer formulation [13] was used to model near-wall effects.

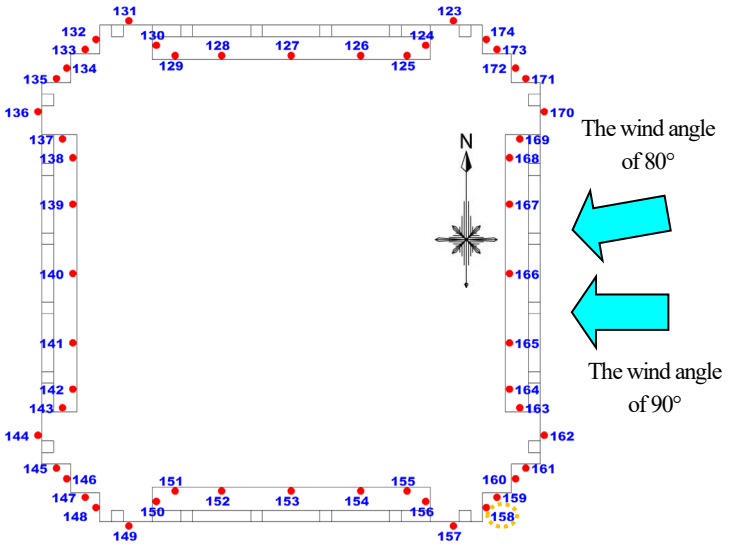

(a) Plan at z = 108.2 m (0.85H) with double corner recesses
(34th floor, Wind pressure measurement point No. 158, to be discussed later)

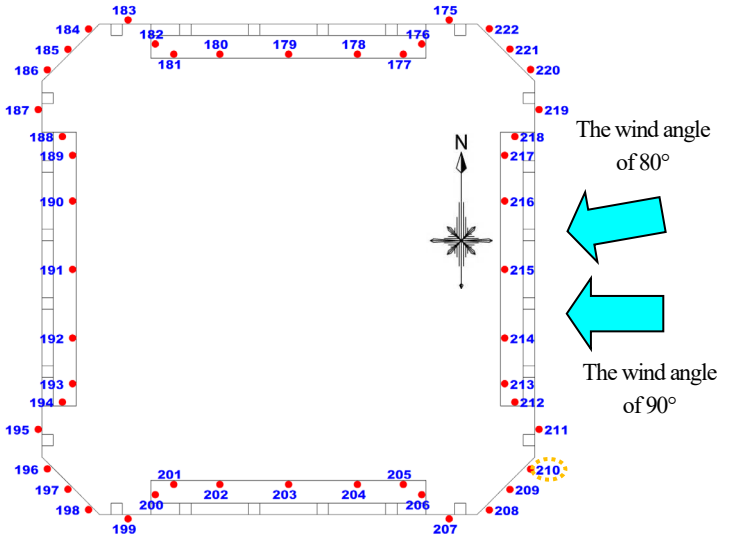

(b) Plan at z = 94.2 m (0.74H) with chamfered corners
(26th floor, Wind pressure measurement point No. 210, to be discussed later)

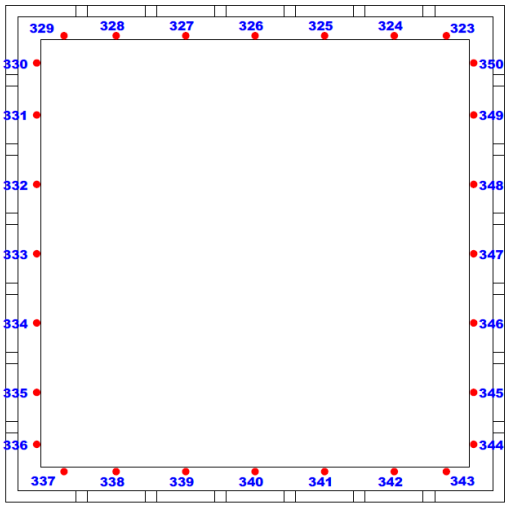

(c) Plan at z =41.7 m (0.33H) with wraparound outer balcony (11th floor)

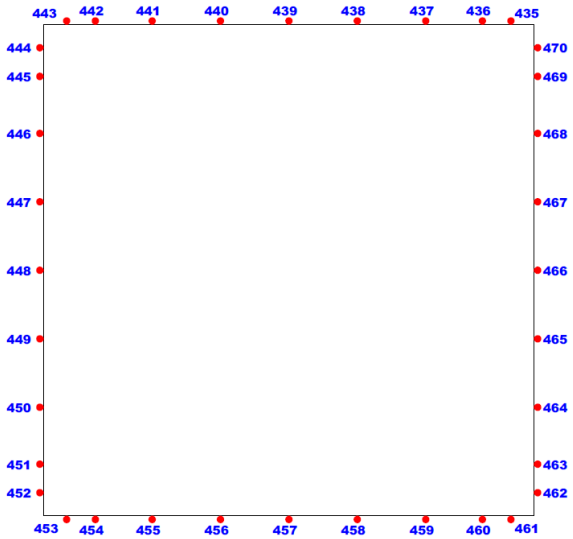

(d) Plan at z =2m (0.16H) with wraparound outer balcony (1st floor)

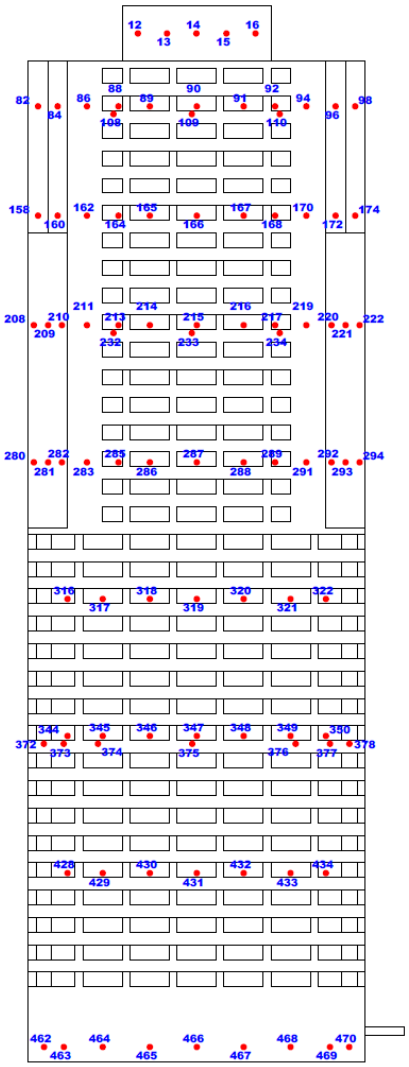

(e) Eastern elevation

Fig. 2. Pressure measurement points on the plan and the eastern elevation of the high-rise residential building.

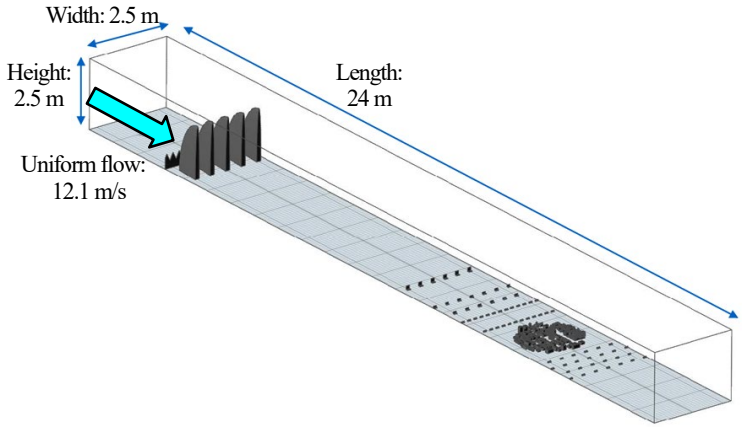

Fig. 3. Wind tunnel model.

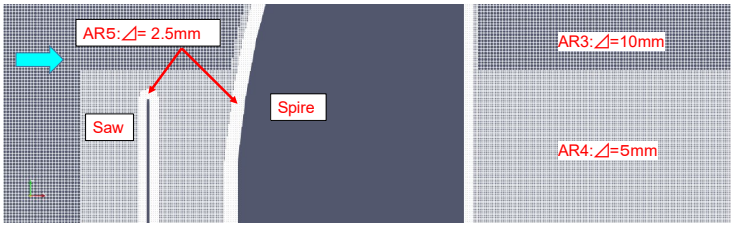

(a) Central cross-section showing turbulence-generating devices (spires and barriers)

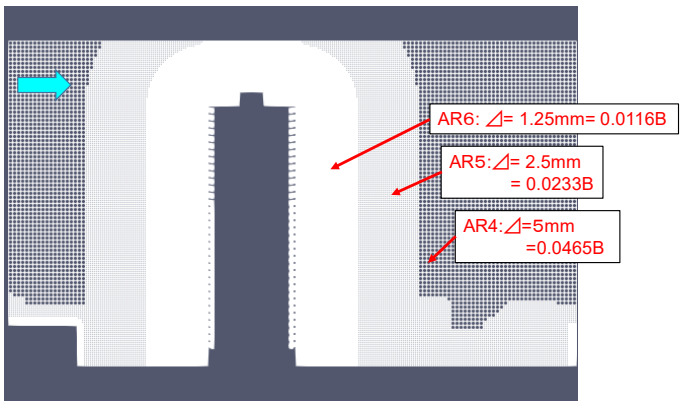

(b) Central cross-section around the high-rise residential building

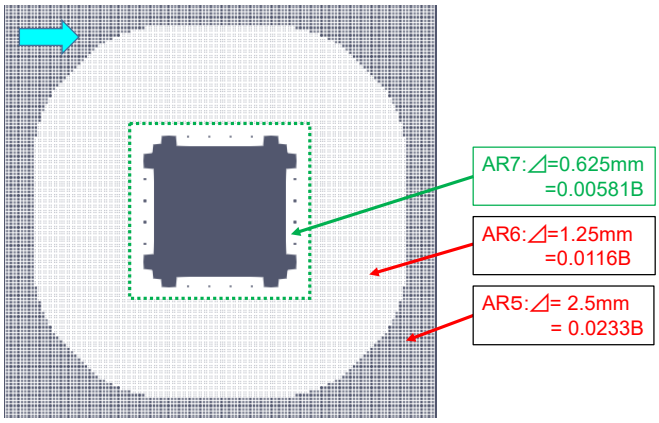

(c) Horizontal section at $z = 270$ mm ($0.84H$) for a wind direction of 90°

Fig. 4. Grid distribution around the high-rise residential building and turbulence-generating devices (90° wind direction) generation (Spier and Saw).

4. Computational conditions

The computational grid used in the domain is shown in Figure 4[14]. The maximum grid spacing in the upper region of the domain, away from the wind tunnel floor, was set to 0.08 m ($0.744B$). In contrast, a minimum grid spacing of 0.625 mm ($0.00581B$) was applied to the surface of the high-rise residential building, where accurate prediction of the wind pressure coefficients is required. This corresponds to a refinement level of seven relative to the maximum grid spacing. The minimum grid spacing is approximately half of the recommended value (B/100), as specified in the CFD Application Guidelines [1]. The refined grid was applied not only within the near-wall boundary layer region but also over an extended region surrounding the building, because accurately simulation of the localized flow separation and reattachment near the windward corners, which have geometric features such as corner recesses and chamfered edges, is required. Conversely, to simulate the turbulence in a neutral atmospheric boundary layer using flow-conditioning devices (e.g., spires, roughness blocks, and barriers) in the wind tunnel, the grid spacing on the devices was set to 2.5 mm ($0.0233B$), which corresponds to a refinement level of five relative to the maximum grid spacing.

To confirm the simulated statistics of the turbulent boundary layer approaching the high-rise residential building in an urban area, additional LBM simulations were conducted for the empty wind tunnel, i.e., without

the high-rise residential building and the surrounding urban area. Table 1 summarizes the computational cases and grids employed in this study.

For the boundary conditions, a uniform inflow velocity was prescribed at the inlet, as described above, with a zero streamwise pressure gradient. The wind tunnel sidewalls and ceiling were modeled using slip-wall boundary conditions. At the outlet, the pressure was fixed to zero, and a zero-gradient condition was imposed on the velocity field. The time step for the LBM simulations was set to $6.11*10^{-4}$ s (corresponding to 1637 Hz) for both configurations, with and without the building model.

To accelerate the computations and address memory constraints associated with the large number of grid points, the simulations were performed using a Linux workstation equipped with a 26-core Intel Skylake CPU and eight NVIDIA Tesla V100-SXM2-16GB GPUs interconnected via NVLink. The LBM simulation of the building-included model (Table 1), comprising approximately 269 million voxels, required about 96 GB of GPU memory. The simulation of 45 s of wind tunnel–scale flow, corresponding to approximately 74,000 time-steps and yielding statistical data equivalent to 50 min at full scale, required approximately 84 h of wall-clock time, including auxiliary computations.

Table 1 Computational cases and grid information

Computational Case	Building Model Included	Refinement Levels	Grid Spacing (mm)	Number of Voxels
Wind tunnel flow (empty domain)	No	0–5	80–2.5	229,210,000
Wind direction: 90°	Yes	0–7	80–0.625	269,000,000
Wind direction: 80°	Yes	0–7	80–0.625	269,400,000

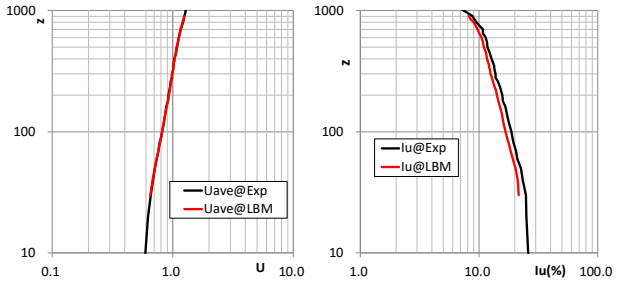

(a) Mean of u (b) Turbulence intensity of u

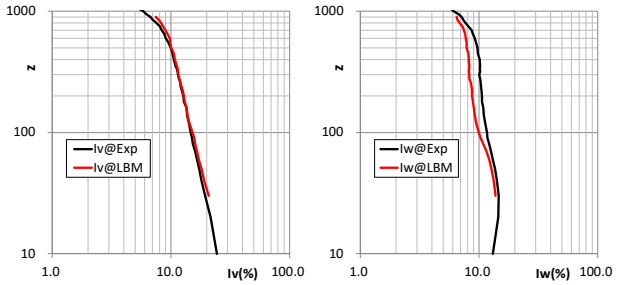

(c) Turbulence intensity of v (d) Turbulence intensity of w

Fig. 5. Vertical profiles of approaching flow at 1-m upstream of the turntable center (without building models).

5. Characteristics and reproducibility of inflow air

To confirm the simulated statistics of the turbulent boundary layer approaching the high-rise residential building in an urban area, Figure 5 shows the vertical profiles of the mean streamwise velocity and the turbulence intensity in the streamwise (u), the spanwise (v) and the vertical (w) velocities at a location 1-m upstream of the building center, corresponding to the upstream edge of the surrounding building model. All velocities are normalized by the reference wind velocity at the height of the high-rise residential building's roof.

The LBM results for the mean wind velocity and spanwise turbulence intensity show good agreement with the experimental data. However, the streamwise turbulence intensity is slightly underestimated, while the vertical turbulence intensity is also lower than the experimental values. At the model roof height of 0.32m, the streamwise turbulence intensity predicted by LBM is 12.4%, which is approximately 91% the size of the experimental value of 13.6% obtained from the wind tunnel measurements.

Figure 6 shows the power spectral density functions of the three velocity components at the height of the model roof, as measured at a location 1-m upstream of the building center, which corresponds to the upstream edge of the surrounding building model. The LBM results underestimate the spectral energy of the *u*- and *w*-components within the low-frequency range (nondimensional frequency $fB/U_H < 0.02$). This underestimation is consistent with the underestimation of turbulence intensities shown in (b) and (d) of Figure 5. One possible cause of this discrepancy is the turbulence generation mechanism within the wind tunnel. Since turbulence is primarily generated by flow-conditioning devices (e.g., spires and roughness elements), insufficient grid resolution near these geometries may lead to inadequate representation of flow separation and subsequent turbulence generation. The LBM reproduces the spectral energy of the *u*- and *w*-components in the higher-frequency range (nondimensional frequency $fB/U_H > 0.02$) and the *v*-component is in reasonable agreement with the experimental data. The present computational approach is expected to be effective for generating inflow turbulence for wind-resistant design.

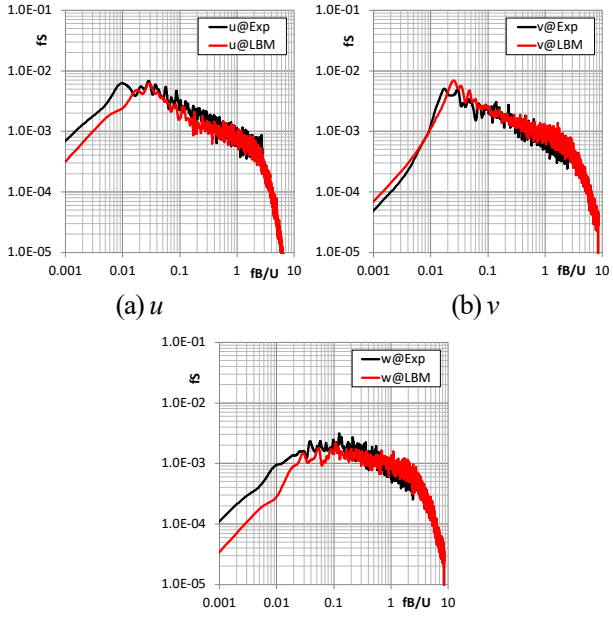

(a) *u* (b) *v*

(c) *w*

Fig. 6. Power spectral density of velocity components at $z = 0.32$ m, 1-m upstream of the building center.

6. Reproducibility of wind pressure coefficients

From this point forward, the results of LBM simulations including both the high-rise residential building model and the surrounding low- and mid-rise building models in the computational domain are discussed. Computational wind pressure coefficients were evaluated at the locations corresponding to the experimental measurement points (e.g., roof and wall surfaces). The wind pressure coefficients were normalized by the dynamic pressure based on the reference velocity measured at the height of the model roof (0.32 m) and at a location 1-m upstream of the building center (i.e., at the upstream edge of the surrounding building model).

The results for wind directions of 90° and 80° are presented in Figures 7 and 8, respectively. The wind direction of 80° was selected, because the magnitude of the minimum peak wind pressure coefficient is maximized at the windward corner on the 26th and the 34th floors in the previous wind tunnel experiments [5].

The mean, the standard deviation and the maximum and minimum peak values of the wind pressure coefficient by means of LES are compared with those of wind tunnel tests in Figures 7 and 8, which obtains experimental data plotted on the horizontal axis and LBM results on the vertical axis. Data points lying on the line with slope 1 indicate exact agreement between the experimental and LBM results.

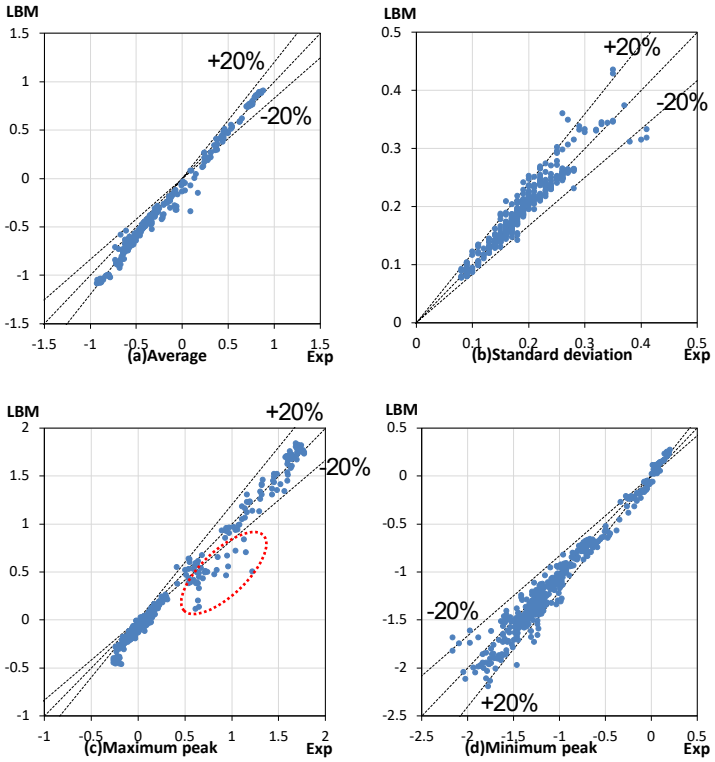

Fig. 7. Comparison of wind pressure coefficients between LBM and experiments (wind direction: 90°).

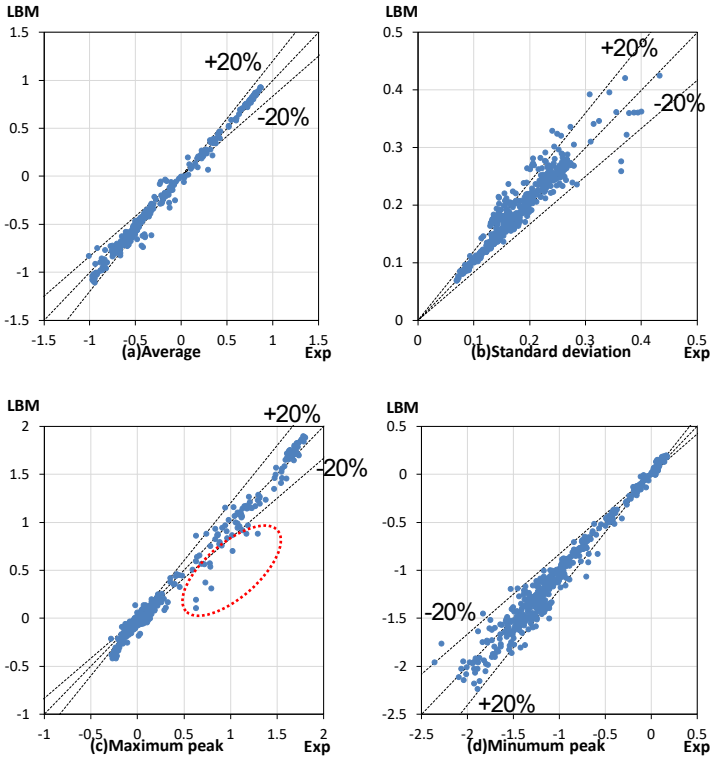

Fig. 8. Comparison of wind pressure coefficients between LBM and experiments (wind direction: 80°).

For the maximum positive values of the mean wind pressure coefficients in Figures 7 and 8, the LBM results closely reproduce the experimental data, indicating that the mean pressure at the stagnation point is accurately captured. Overall, the mean values, standard deviations and maximum and minimum peak wind pressure coefficients predicted by LBM fall within ±20% of the experimental results (i.e., within the region bounded by

the dotted lines in Figures 7 and 8), demonstrating the validity of the LBM predictions.

However, for some measurement points, the LBM underestimates the maximum peak wind pressure coefficient, which experimentally ranges from 0.5 to 1.2, as indicated by the red dashed line of Figure 7(c) and 8(c). These measurement points are located on the wall parallel to the windward wall (east wall) within corner recesses and on at the windward corners of walls inside balconies on lower floors.

7. Distributions of wind pressure coefficients along the wall surface with various wind directions

This section presents the circumferential distribution of wind pressure coefficients on the wall surfaces at representative measurement heights of 34th, 26th, 11th and 2nd floors (see Figures 9 and 10). The goal is to evaluate the ability of LBM to reproduce the spatial distribution of wind pressure due to the slight change in wind direction from 90° to 80°.

The characteristic variation in the mean, standard deviation, maximum and minimum of the peak wind pressure coefficients computed by LBM shows quite good agreement with the experimental results, except in below some areas near the windward corner.

Firstly, we focus on the double corner recession at the windward corner of the 34th floor (east wall) in region A of Figure 9(a) and region C of Figures 10(a) respectively. Considering that the mean pressure of the measurement point No. 158 is larger than that of No. 160 and that the standard deviation of pressure at No. 158 is larger than that of No. 160, it is found that the separated shear layers from the frontal wall at the southeast corners reattach to the recessions of the leeward corner as indicated by the green arrows in Figure 9(a) and Figure 10(a). The variation in pressure characteristics of the mean and the standard deviation from the LBM matched the experimental results. However, LBM underestimates the maximum peak pressure of No. 158 at 90° and the absolute values of minimum peak pressure of No. 158 at 80°. It is supposed that LBM did not provide a sufficient grid resolution to capture the separated flow and the reattachment of flow occurring within the doble corner recesses.

Secondly, we focus on the windward chamfered corners at 26th floor in region B of Figure 9(b) and region D of Figure 10(b) respectively. Considering that the mean pressure of the measurement point No. 210 is smaller than those of No. 208 and No. 209 and that the standard deviation of pressure at No. 210 is quite larger than those of No. 208 and No. 209, it is expected that fast circulating flow locally occurs at the windward chamfered corner on No. 210 as indicated by the green arrows in Figure 9(b) and Figure 10(b). LBM underestimates both the standard deviation and the magnitude of the minimum peak value of No. 210, because the local vortical flow at the windward chamfered corners could not be resolved computationally due to the coarse mesh.

Except at the windward corner regions of the 34th and 26th floors, the wind pressure coefficients on the building wall surfaces are generally well reproduced in comparison with the experimental results. In particular, the pressure coefficients on the wall surface near the balconies on the 11th floor and on the first-floor wall surfaces enclosed by the surrounding building blocks can be precisely reproduced by LBM.

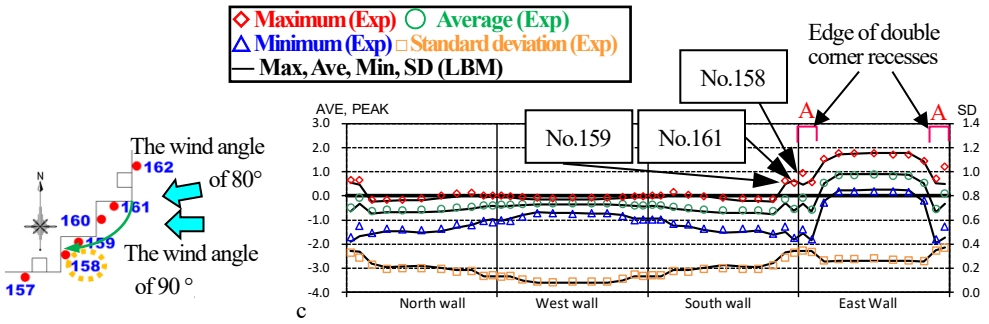

(a)34th floor (z = 108.2 m) with double corner recesses

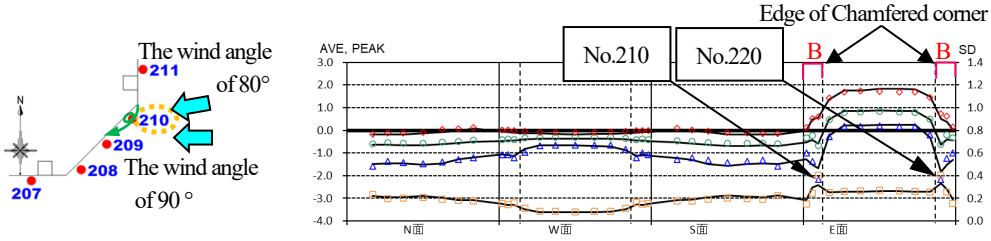

(b)26th floor (z = 94.2 m) with chamfered corners

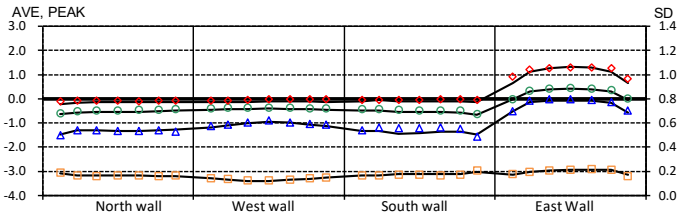

(c)11th floor (z = 41.7 m) with external balconies

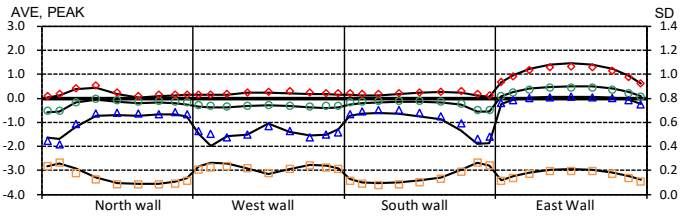

(d)1st floor (z = 2 m) with right-angle corners

Fig. 9. Wall pressure distribution on the high-rise residential building (wind direction: 90°, H = 128 m).

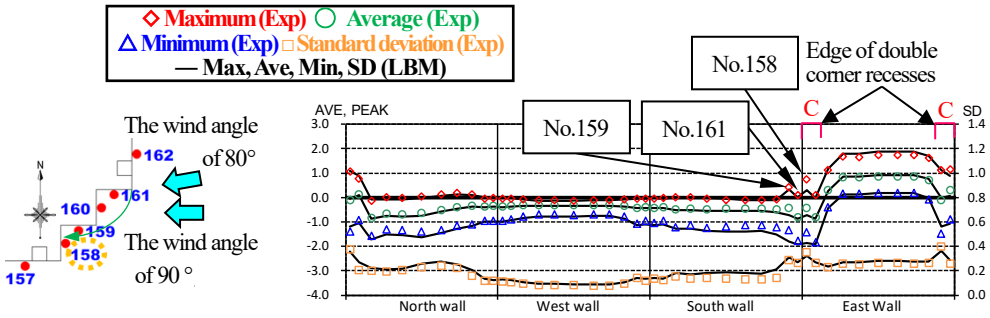

(a) 34th floor (z = 108.2 m) with double corner recesses

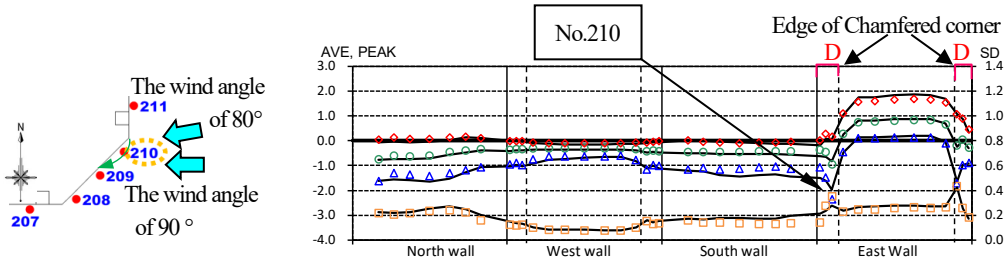

(b) 26th floor (z = 94.2 m) with chamfered corners

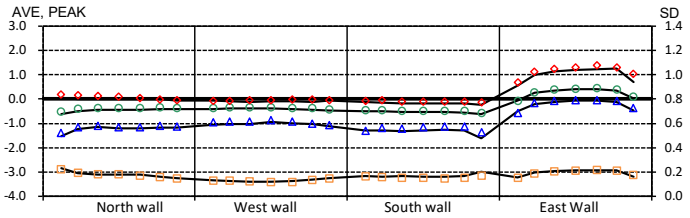

(c) 11th floor (z = 41.7 m) with external balconies

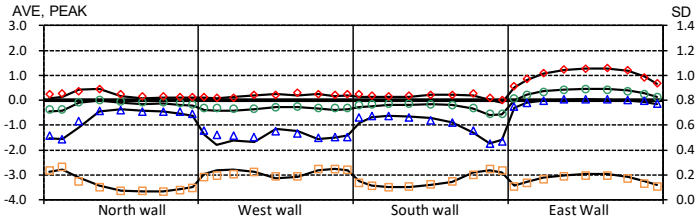

(d) 1st floor (z = 2 m) with right-angle corners

Fig. 10. Wall pressure distribution on the high-rise residential building (wind direction: 80°, H = 128 m).

8. The dynamic characteristics of the wind pressure at the windward corners

The magnitude of the minimum peak wind pressure coefficient is maximized at the southeast corners of the 26th and the 34th floors in case of the wind direction of 80° as shown in the previous seventh section. In this section we investigate the power spectral density of the measurement points No. 158 and No. 210 in Figures 11 and 12.

In case of 90° at No. 158 in the double corner recesses, the minimum peak pressure of LBM in Figure 9(a) is good agreement with the that of the experiment. The power spectral density of LBM is also good agreement with the that of the experiment as shown in Figure 11(a). On the other hand, in case of 90° at No. 158, the magnitude of minimum peak pressure and the standard deviation of LBM in Figure 10(a) is smaller than those of the experiment. Although the spectral energy in the high-frequency range ($fB/U_H > 0.1$) is well reproduced by the LBM, the spectral energy in the low-frequency range ($fB/U_H < 0.02$) is underestimated.

Thus, the occurrence of underestimation of the absolute value of the minimum peak wind pressure coefficient and insufficient low-frequency components of the PSD of the wind pressure coefficient at the same time in LBM is observed in case of chamfered corners at both 80° and 90° as shown in Figure 12.

As the future work, we intend to focus our analysis on the relationship between the reproduction of the minimum peak wind pressure coefficient and the reproduction of the low-frequency components of the wind pressure coefficient.

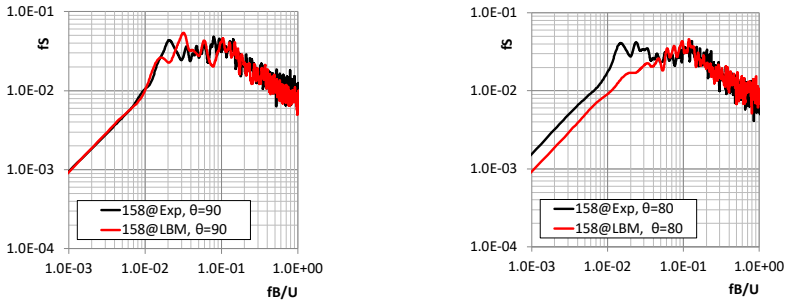

(a)Wind direction of 90 degree (b)Wind direction of 80 degree

Fig. 11. Power spectral density of pressure coefficients of Measurement point No. 158 in the double corner recesses of 34F

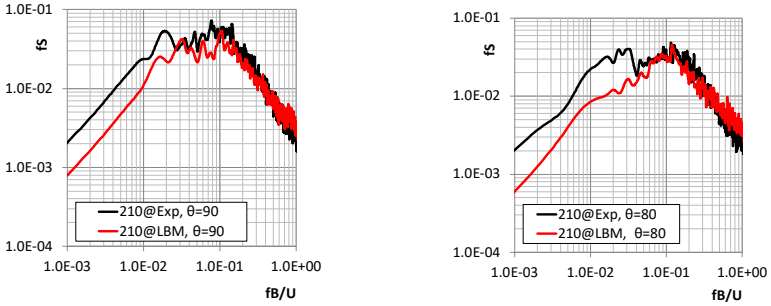

(a)Wind direction of 90 degree (b)Wind direction of 80 degree

Fig. 12. Power spectral density of pressure coefficients of Measurement point No. 210 in the chamfered corners of 26F

9. Conclusion

In this study, wind pressure coefficients acting on a high-rise residential building located within a low- and mid-rise urban area were predicted using LES based on the cumulant Lattice Boltzmann formulation with the D3Q27 model. The numerical framework incorporates a subgrid-scale model equivalent to the standard Smagorinsky model, an immersed boundary method with wall modeling, and a Cartesian mesh with octree-based grid refinement.

By explicitly modeling turbulence-generating devices (e.g., spires and roughness elements) in the wind tunnel, the inflow turbulence generated by the LBM reproduces the mean wind velocity and turbulence intensity in reasonable agreement with the experimental results. However, analysis of the power spectral

density of the velocity field indicates that the LBM slightly underestimates the spectral energy of the streamwise and vertical velocity components in the low-frequency range ($fB/U_H < 0.02$) compared with the wind tunnel data.

It is confirmed that the mean, standard deviation, and peak wind pressure coefficients of the building predicted by LBM fall within approximately ±20% of the experimental results, demonstrating the validity and engineering applicability of the present approach. Taking into consideration on the relatively short computational time, LES based on LBM can be considered a practical and efficient method for wind engineering applications.

The influence of wind direction on the minimum peak wind pressure coefficient at the windward corners of the building (corner recesses and chamfered corners), which are critical regions in wind-resistant design, is qualitatively reproduced but quantitatively underestimated. It is expected that the possible causes include the insufficient spectral energy of generated inflow turbulence in the low-frequency range ($fB/U_H < 0.02$) compared with the experimental data and insufficient grid resolution around the double corner recesses and chamfered corners of the high-rise residential building.

References

[1] Architectural Institute of Japan, Guidebook of Recommendations for Loads on Buildings 2 / Wind-induced Response and Load Estimation / Practical Guide of CFD for Wind Resistant Design, Architectural Institute of Japan, 2017. (in Japanese)

[2] Architectural Institute of Japan, Manual on Wind Loading Estimation by CFD, Architectural Institute of Japan, 2024. (in Japanese)

[3]T. Tamura, K. Kondo, H. Kataoka, H. Kikuch, K. Ohtake, H. Terasaki, Y. Yoshie, H. Kawai, M. Tsubokura, Implementation report "Study on the introduction of computational fluid dynamics into standards for wind pressure, wind-resistant design, etc.", The Building Letter, No.637, 2019 (in Japanese)

[4]Elisa Buffa , Jerome Jacob, Pierre Sagaut, Lattice-Boltzmann-based large-eddy simulation of high-rise building aerodynamics with inlet turbulence reconstruction, J. Wind. Eng. Ind. Aero. 212 (2021) 104560.https://doi.org/10.1016/j.jweia.2021.104560

[5] Y. Itoh et al., Study on the introduction of computational fluid dynamics into wind-resistant design of buildings, Part 2: Wind tunnel experiments on high-rise office and residential buildings, in: Summaries of Technical Papers of the Annual Meeting, Architectural Institute of Japan, 2016, pp. 235–236. (in Japanese)

[6] Architectural Institute of Japan, Recommendations for Loads on Buildings (2015), Architectural Institute of Japan, 2015. (in Japanese)

[7]Altair Engineering, ultraFluidX product page. https://help.altair.com/hwcfdsolvers/ufx/index.htm

[8] C.A. Niedermeier, C.F. Janben, T. Indinger, Massively-parallel multi-GPU simulations for fast and accurate automotive aerodynamics, in: Proceedings of the 6th European Conference on Computational Mechanics (ECCM 6) and 7th European Conference on Computational Fluid Dynamics (ECFD 7), 2018.

[9] M. Geier, M. Schönherr, A. Pasquali, M. Krafczyk, The cumulant lattice Boltzmann equation in three dimensions: Theory and validation, Comput. Math. Appl. 70 (2015) 507–547. https://doi.org/10.1016/j.camwa.2015.05.001.

[10] M. Geier, A. Pasquali, M. Schönherr, Parametrization of the cumulant lattice Boltzmann method for fourth order accurate diffusion Part I: Derivation and validation, J. Comput. Phys. 348 (2017) 862–888. https://doi.org/10.1016/j.jcp.2017.05.040.

[11] M. Geier, A. Pasquali, M. Schönherr, Parametrization of the cumulant lattice Boltzmann method for fourth order accurate diffusion Part II: Application to flow around a sphere at drag crisis, J. Comput. Phys. 348 (2017) 889–898. https://doi.org/10.1016/j.jcp.2017.07.004.

[12] O. Malaspinas, P. Sagaut, Consistent subgrid scale modelling for lattice Boltzmann methods, J. Fluid Mech. 700 (2012) 514–542. https://doi.org/10.1017/jfm.2012.155.

[13] O. Malaspinas, P. Sagaut, Wall model for large-eddy simulation based on the lattice Boltzmann method, J. Comput. Phys. 275 (2014) 25–40. https://doi.org/10.1016/j.jcp.2014.06.020.

[14] Y. Itoh, K. Kondo, T. Tamura, K. Ijuin, Numerical prediction of wind pressure around a high-rise residential building in urban area by means of LES based on lattice Boltzmann method, in: Proceedings of the symposium on computational fluid dynamics E06-4, 2020 (in Japanese)